Optical Imaging Through Clouds and Fog

Sermsak Jaruwatanadilok, Akira Ishimaru, *Life Fellow, IEEE*, and Yasuo Kuga, *Senior Member, IEEE*

***Abstract*—Imaging and detection of objects at optical wavelengths offers better resolution than at microwave or millimeter wavelengths. However, the imaging is severely affected by scattering from fog and clouds. This paper presents a study of optical imaging through clouds by using the point-source vector radiative transfer theory. The point-spread function including complete polarization characteristics is presented with numerical examples at 1 μm wavelength showing the effects of aperture size and optical depth on the shower curtain effects.**

***Index Terms*—Optical imaging, optical propagation in random media, optical scattering, point source, point spread function, radiative transfer.**

I. Introduction

THE IMAGING and detection of objects through the atmosphere is an important problem of current interest. Optical imaging offers much better resolution than microwave or millimeter wave. However, the optical propagation is severely affected by fog and clouds in the atmosphere. This paper presents the imaging of objects through clouds and fog at a wavelength of 1 μm. The total distance between the object and the imaging system is 20 km, and the fog or cloud thickness is 1 km.

If the optical depth is much smaller than one, the single-scattering approximation can be used. However, light suffers considerable scattering at large optical depth, thus, the diffusion approximation is often used. In many practical situations, the optical depth value is somewhere in between; therefore, neither the single-scattering nor the diffusion approximations may be appropriate. In this paper, we employ the complete vector radiative transfer theory which is applicable to any optical depth and any polarization state.

For the imaging problem, we need to consider the radiative transfer equation with a point-source. However, this Green's function problem has not been solved yet. We present an approximate solution to this problem, making use of the plane-wave solution to the radiative transfer equation. Note that we derive the full vector radiative transfer equation in this paper even though we only use the intensity information in our calculations. Our derivations are intended to be in a general form for use in the future because polarization information is very useful and can be exploited to improve the quality of the images.

The solution to the point-source radiative transfer is then used in the optical system to derive the point spread function. The image at the imaging plane and the resolution are studied in terms of the optical depth, the aperture size, and whether the location of the fog is close to the object or close to the imaging system. In this connection, we also discuss an important phenomenon called *shower curtain effect*. The shower curtain effect has been recognized in the applications of imaging through random media for several years. It states that, in addition to the properties of the random medium, the location of the random medium also affects the image qualities. In a situation where the properties of the random medium, i.e., concentration of the scattering particles and the actual length of the medium, are fixed, the image qualities when the random medium is close to the object are better than the image qualities when the random medium is close to the observer. In an everyday situation, we will see a person behind the shower curtain better than that person sees us, which is the source of the name *shower curtain effect*.

There are several studies related to the shower curtain effect. Belov and Borisov [1] discussed *T-Effect* and shower curtain effect. They showed that the image qualities decrease nonmonotonically as a function of the distance from the object to the random medium. However, they concluded that this characteristic depends not only on the properties of the scattering medium and the location of the medium but also on the spatial structure of the radiation properties of the object. In our calculations, we apply the concept of the point spread function. The images are the result of the convolution of the object intensity with the point spread function of the optical system including the effect of the random medium. The counterpart of the point spread function is the modulation transfer function concept. Basically, they are a Fourier transform pair in spatial domain. The modulation transfer function (MTF) of layered inhomogeneous random media was calculated [2], [3]. Several experiments were performed to verify the shower curtain effect [2], [4]. Most of this shower curtain effect is studied under the circumstances of atmospheric imaging. However, the shower curtain effect has recently been considered in the context of optical coherence tomography, which applies to biomedical imaging [5], [6].

We present the vector radiative transfer equation for the point-source function in Section II. We explain the approximation made from the plane-wave radiative transfer equation and the limitations of this modified equation. Section III shows the analysis of the imaging system. The point spread functions are calculated for various optical depths and aperture sizes. The shower curtain effect is presented in terms of point spread function broadening and the imaging of a cross pattern. Our conclusions are in Section IV.

II. Point-Source Vector Radiative Transfer Equation

In this section, we first start with the vector radiative transfer equation in the general form. Then, we derive the formulation

Manuscript received August 7, 2002; revised March 19, 2003. This work was supported by the National Science Foundation under Grant ESC-9908849, by the Office of Naval Research under Grant N000140010027, and by the U.S. Air Force Research Laboratory under Grant F29601-00-C-0240.

The authors are with the Department of Electrical Engineering, University of Washington, Seattle, WA 98195 USA (e-mail: sermsak@ee.washington.edu).

Digital Object Identifier 10.1109/TGRS.2003.813845

in the point-source case. With some reasonable assumptions, we are able to apply the method used in solving the vector radiative transfer equation with plane-wave incidence in a plane-parallel problem to this point-source problem.

A. Vector Radiative Transfer Equation

The vector radiative transfer equation in the general form is given by

$$\hat{s}\cdot\nabla\mathbf{I}(r,\hat{s}) = -\rho\sigma_t\mathbf{I}(r,\hat{s}) + \int_{4\pi}\mathbf{S}(\hat{s},\hat{s}')\mathbf{I}(r,\hat{s}')\,d\Omega' + \mathbf{J}(r,\hat{s}) \tag{1}$$

where $\mathbf{I}$ is the modified Stokes vector given by

$$\mathbf{I} = \begin{bmatrix} I_1 & I_2 & U & V \end{bmatrix}^T. \tag{2}$$

ρ is the number density, and σ_t is the total scattering cross section. The matrix $\mathbf{S}$ is the Mueller matrix. The scattering characteristics of the random medium are captured in the Mueller matrix $\mathbf{S}$ defined by

$$\mathbf{S} = \begin{bmatrix} \mathbf{S}_1 & \mathbf{S}_2 \\ \mathbf{S}_3 & \mathbf{S}_4 \end{bmatrix} \tag{3}$$

$$\mathbf{S}_1 = \begin{bmatrix} |f_{11}|^2 & |f_{12}|^2 \\ |f_{21}|^2 & |f_{22}|^2 \end{bmatrix} \tag{3a}$$

$$\mathbf{S}_2 = \begin{bmatrix} \Re(f_{11}f_{12}^*) & -\Im(f_{11}f_{12}^*) \\ \Re(f_{21}f_{22}^*) & -\Im(f_{21}f_{22}^*) \end{bmatrix} \tag{3b}$$

$$\mathbf{S}_3 = \begin{bmatrix} 2\Re(f_{11}f_{21}^*) & 2\Re(f_{12}f_{22}^*) \\ 2\Im(f_{11}f_{21}^*) & 2\Im(f_{12}f_{22}^*) \end{bmatrix} \tag{3c}$$

$$\mathbf{S}_4 = \begin{bmatrix} 2\Re(f_{11}f_{22}^*+f_{12}f_{21}^*) & -2\Im(f_{11}f_{22}^*-f_{12}f_{21}^*) \\ 2\Im(f_{11}f_{22}^*+f_{12}f_{21}^*) & -2\Re(f_{11}f_{22}^*-f_{12}f_{21}^*) \end{bmatrix} \tag{3d}$$

where f_{11}, f_{12}, f_{21}, and f_{22} are the scattering amplitudes calculated using Mie scattering explained in Appendix A [7]. We define the submatrices $\mathbf{S}_1$, $\mathbf{S}_2$, $\mathbf{S}_3$, and $\mathbf{S}_4$ for the derivation in the next subsections. $\mathbf{J}$ is the source vector which is given by

$$\mathbf{J}(r,\hat{s}) = \int_{4\pi}\mathbf{S}(\hat{s},\hat{s}')\mathbf{I}_{ri}(r,\hat{s}')\,d\Omega' \tag{4}$$

where $\mathbf{I}_{ri}$ is the reduced intensity Stokes vector given by

$$\mathbf{I}_{ri}(r,\hat{s},\hat{s}') = \frac{\mathbf{I}_o}{r^2}g(\hat{s}')\exp(-\rho\sigma_t r)\delta(\hat{s}-\hat{s}') \tag{5}$$

where $\mathbf{I}_o$ is the Stokes vector of the source; r is the distance through which light has travelled in the scattering medium; $\hat{s}'$ is the direction of the source incidence; and $\hat{s}$ is the direction of observation. The directional gain function of the source is $g(\hat{s}')$. In the isotropic point-source case, $g(\hat{s}') = 1$. In other types of transmitters (e.g., directional antennas), $g(\hat{s}')$ depends on the direction of propagation. We concentrate on the plane-parallel geometry shown in Fig. 1. Equation (1) becomes

$$\left(\mu\frac{\partial}{\partial\tau}+1\right)\mathbf{I}(\tau,\mu,\phi) = \int_0^{2\pi}\int_{-1}^{1}\mathbf{S}(\mu,\phi,\mu',\phi') \cdot\mathbf{I}(\tau,\mu',\phi')\,d\mu'\,d\phi' + \mathbf{J}(\tau,\mu,\phi), \quad \text{for } 0\le\tau\le\tau_o \tag{6}$$

where $\mu = \cos\theta$, $\tau = \rho\sigma_t z$ is the *optical distance*, and $\tau_o = \rho\sigma_t L$ is the *optical depth*.

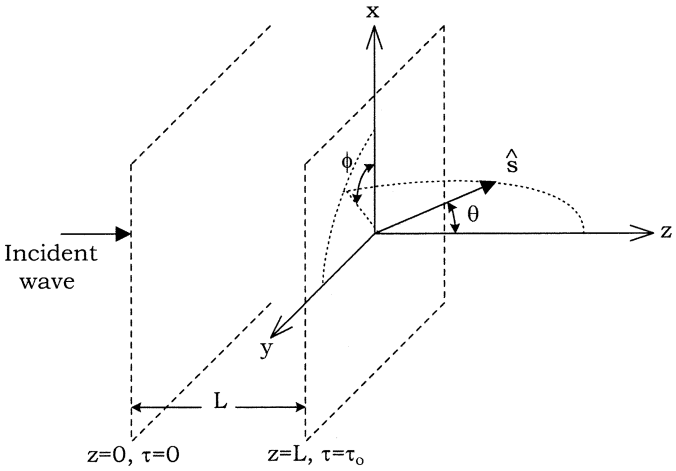

Fig. 1. Plane-parallel geometry.

We assume that the only source of radiation is the incident wave; therefore, the boundary conditions in this problem can be written as

$$\begin{aligned} \mathbf{I}(\tau=0) &= 0, \qquad \text{for } 0\le\mu\le 1 \\ \mathbf{I}(\tau=\tau_o) &= 0, \qquad \text{for } -1\le\mu\le 0. \end{aligned} \tag{7}$$

The source vector is given by

$$\mathbf{J}(\tau,\mu,\phi) = \int_0^{2\pi}\int_{-1}^{1}\mathbf{S}(\mu,\phi,\mu',\phi')\mathbf{I}_{ri}(\tau,\mu',\phi')d\mu'd\phi'. \tag{8}$$

For the plane-wave case, the reduced Stokes vector is

$$\mathbf{I}_{ri}(\tau,\mu',\phi') = \mathbf{I}_o\exp(-\tau)\delta(\mu'-1)\delta(\phi'). \tag{9}$$

However, for a point-source or transmitter with directional gain, represented by (5), the formulation shown in (6) is not easily solved. Previously, we reported on the plane-wave radiative transfer equation in the plane-parallel problem [8]. With some assumptions and approximations, we find that we can modify the previous procedures to solve for the vector radiative transfer equation in (6). In the next section, we discuss these assumptions and approximations.

B. Approximation to the Point-Source Radiative Transfer Equation

In contrast to the plane-wave incidence where the reduced Stoke vector of the source propagates in only one direction, the reduced Stokes vector for the point-source case propagates in different directions. All the reduced Stokes vectors from those directions contribute to the final results of the radiative transfer equation. Furthermore, the reduced intensity is not a simple function of τ and μ, but rather a function of spherical coordinates r, θ, and μ [9]. Therefore, the exact and complete formulation of the point-source case has to be in spherical coordinates, and the variation of the reduced Stokes vector in the source term has to be considered.

We approach the point-source radiative transfer equation from the plane-wave solution with the following assumptions and approximations. Fig. 2 shows the geometry explaining the approximation of point-source incidence from the plane-wave incidence.

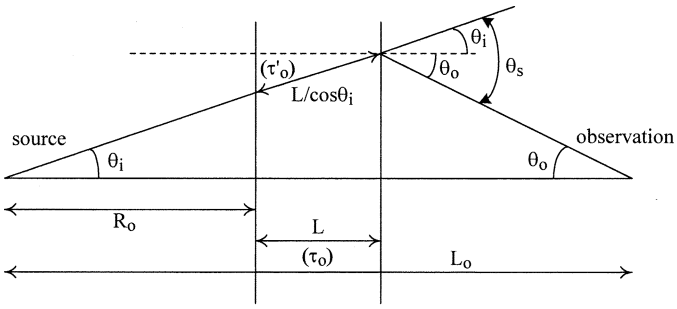

Fig. 2. Point-source consideration geometry.

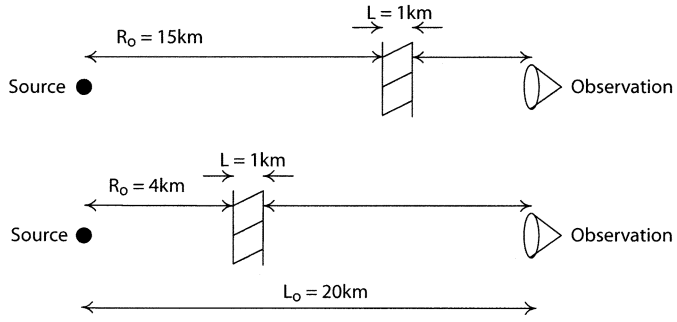

Fig. 3. Geometry of point-source problem.

1) The thickness of the slab of a random medium is small compared to the total distance ($L < L_o$).
2) The off-axis incident Stokes vector is approximated to be normally incident on the slab of random medium and propagates through the random medium with a distance longer than L. This distance increases by a factor of $1/\mu_i$, where $\mu_i = \cos\theta_i$, and θ_i is the incident angle.
3) The result of the point-source radiative transfer at the angle θ_o is the result of the plane-wave radiative transfer equation at the angle θ_s from the incident angle θ_i. The relationship between these angles is given by

$$(R_o + L)\tan\theta_i = [L_o - (R_o + L)]\tan\theta_o \tag{10}$$

$$\theta_s = \theta_o + \theta_i. \tag{11}$$

4) The r dependence from the reduced Stokes vector is embedded in z dependence and can be written as

$$\mathbf{I}_{ri} = \frac{\mathbf{I}_o}{\left[\frac{(R_o+z)}{\mu}\right]^2} g(\mu)\exp(-\tau)\delta(\mu'-1)\delta(\phi') = \frac{\mathbf{I}_o}{\left(\frac{R_o}{\mu}\right)^2\left[1+\left(\frac{z\mu}{R_o}\right)\right]^2} g(\mu)\exp(-\tau)\delta(\mu'-1)\delta(\phi'). \tag{12}$$

This approximation is valid when the first assumption holds. However, (12) cannot be incorporated directly into the equation because of z dependence. We make an approximation of this z dependence in the fraction form to the exponential form by

$$\frac{1}{\left[1+\left(\frac{z\mu}{R_o}\right)\right]^2} \equiv \frac{1}{(1+\Delta)^2} \approx \exp(-\alpha\Delta) \tag{13}$$

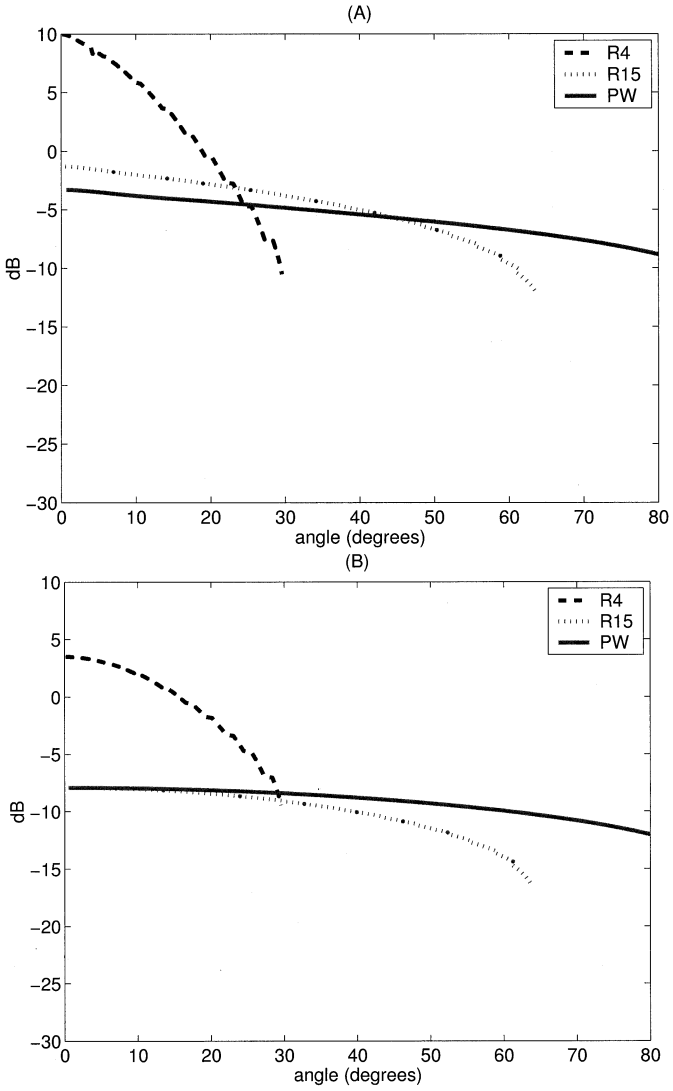

Fig. 4. Comparison of angular spectrum between point-source and plane-wave incidences when (A) optical depth is 10 and (B) optical depth is 20.

TABLE I
PARTICLE SIZE DISTRIBUTION OF FOG

Diameter of Particle (μm)	Number of particles
0.4	3
0.6	10
0.7	40
1.4	50
2.0	7
3.6	1
5.4	9
8.0	2

where α is given by solving (13) with equality at $\Delta = L/R_o$

$$\alpha = 2\left(\frac{R_o}{L}\right)\log_e\left[1+\frac{L}{R_o}\right]. \tag{14}$$

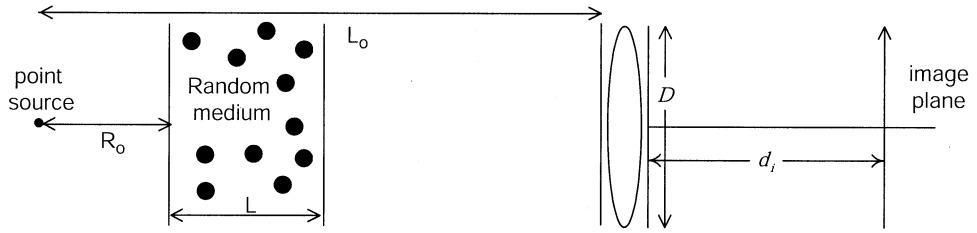

Fig. 5. An imaging system.

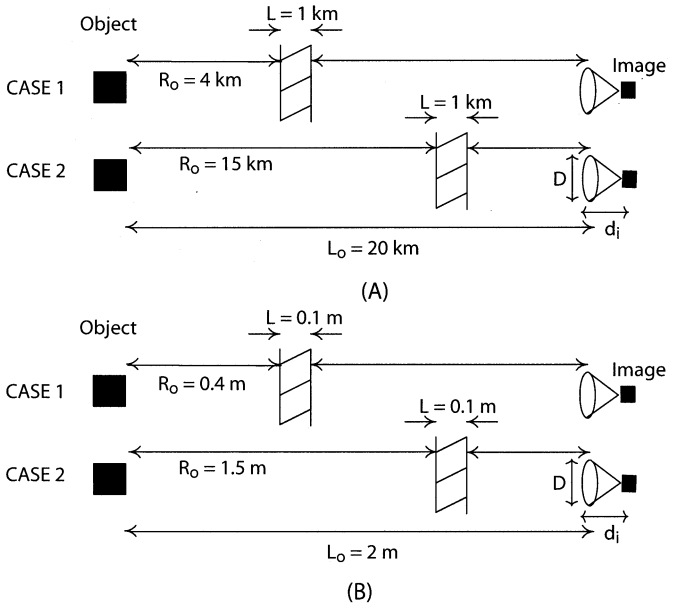

Fig. 6. Imaging geometry. (a) Large distance and small angle. (b) Small distance and large angle.

Thus, (12) becomes

$$\mathbf{I}_{ri} = \frac{\mathbf{I}_o}{\left(\frac{R_o}{\mu}\right)^2} g(\mu) \exp\left[-\left(1+\frac{\alpha\mu}{\rho\sigma_t R_o}\right)\tau\right] \delta(\mu'-1)\delta(\phi'). \tag{15}$$

5) We find the solution of the point-source vector radiative transfer for angle θ_o at the observation point by solving the approximate plane-wave normally incident to the plane-parallel medium with a slant path $L/\cos(\theta_i)$ (equivalent to optical depth of τ_o'). The reduced Stokes vector in (15) is used in this case.

Now, we use (15) as the reduced Stokes vector for (8) and then plug it into the vector radiative transfer (6). The solution procedure is explained in the following section. Note that it is the same as for the plane-wave incident case [8].

C. Solution to the Vector Radiative Transfer Equation

To solve (6), we first expand the azimuthal dependence using the Fourier series. Thus, the Stokes vector becomes

$$\mathbf{I}(\tau,\mu,\phi) = \mathbf{I}^{(0)}(\tau,\mu) + \sum_{n=1}^{\infty}\left[\mathbf{I}_{dc}^{(n)}(\tau,\mu)\cos(n\phi) + \mathbf{I}_{ds}^{(n)}(\tau,\mu)\sin(n\phi)\right]. \tag{16}$$

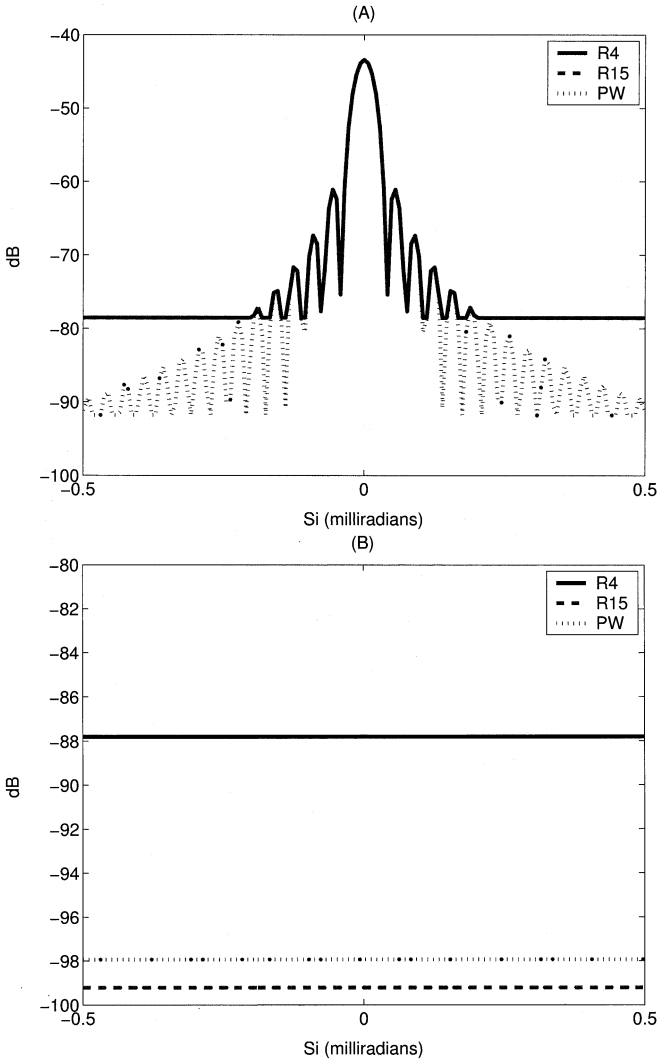

Fig. 7. One-dimensional cut from 2-D point spread function for large distance geometry. (a) Optical depth $= 10$. (b) Optical depth $= 25$.

Different cases of incident polarization (linear or circular) can be considered separately. In this paper, we consider only circular polarization where $\mathbf{I}_o = [1/2 \quad 1/2 \quad 0 \quad 1]^T$. In this case, the only nonzero mode is mode zero. Note that this is true only when the approximation in assumption 2 in the previous subsection holds. In nonnormal incident case, the Fourier series expansion gives more terms resulting in more calculation time. However, except for the first few terms, the contribution of the Fourier expansions is expected to be small. Equation (6) can be reduced to two uncoupled equations, which gives a faster solution time.

The two uncoupled equations are the I_1I_2 equation and the UV equation. The I_1I_2 equation is given by

$$\left(\mu\frac{\partial}{\partial\tau}+1\right)\mathbf{I}^{(0)}_{I_1I_2}(\tau,\mu)=\int_{-1}^{1}\mathbf{L}^{(0)}_{1}(\mu,\mu')\mathbf{I}^{(0)}_{I_1I_2}(\tau,\mu')\,d\mu' +\mathbf{F}^{(0)}_{I_1I_2}(\mu)\exp(-\alpha\tau),\ \text{for } 0\le\tau\le\tau'_o \quad (17)$$

where

$$\mathbf{I}^{(0)}_{I_1I_2}(\tau,\mu)=\begin{bmatrix}I^{(0)}_1(\tau,\mu,)\\ I^{(0)}_2(\tau,\mu,)\end{bmatrix} \quad (18)$$

$$\mathbf{F}^{(0)}_{I_1I_2}(\mu)=\frac{g(\mu)}{2\sigma_t\left(\frac{R_o}{\mu}\right)^2}\begin{bmatrix}|A_{ll}(\mu)|\\ |A_{rr}(\mu)|\end{bmatrix} \quad (19)$$

$$\mathbf{L}^{(0)}_{1}(\mu,\mu')=\int_0^{2\pi}\mathbf{S}_1(\mu,\mu',\phi'-\phi)\,d(\phi'-\phi). \quad (20)$$

The UV equation is expressed as

$$\left(\mu\frac{\partial}{\partial\tau}+1\right)\mathbf{I}^{(0)}_{UV}(\tau,\mu)=\int_{-1}^{1}\mathbf{L}^{(0)}_{4}(\mu,\mu')\mathbf{I}^{(0)}_{UV}(\tau,\mu')\,d\mu' +\mathbf{F}^{(0)}_{UV}(\mu)\exp(-\alpha\tau),\ \text{for } 0\le\tau\le\tau'_o \quad (21)$$

where

$$\mathbf{I}^{(0)}_{UV}(\tau,\mu)=\begin{bmatrix}U^{(0)}(\tau,\mu)\\ V^{(0)}(\tau,\mu)\end{bmatrix} \quad (22)$$

$$\mathbf{F}^{(0)}_{UV}(\mu)=\frac{g(\mu)}{\sigma_t\left(\frac{R_o}{\mu}\right)^2}\begin{bmatrix}-\Im[A_{ll}(\mu)A^*_{rr}(\mu)]\\ \Re[A_{ll}(\mu)A^*_{rr}(\mu)]\end{bmatrix} \quad (23)$$

$$\mathbf{L}^{(0)}_{4}(\mu,\mu')=\int_0^{2\pi}\mathbf{S}_4(\mu,\mu',\phi'-\phi)\,d(\phi'-\phi). \quad (24)$$

The functions A_{ll} and A_{rr} are defined in Appendix A.

We solve this integrodifferential equation using the discrete ordinates method. It is based on applying the Gauss quadrature formula [11] of order N in μ dependence to (18) and (22). The integrodifferential equation of (18) and (22) becomes a first-order differential equation in the form

$$\frac{\partial}{\partial\tau}\mathbf{I}+\mathbf{A}\mathbf{I}=\mathbf{B}\exp(-\alpha\tau) \quad (25)$$

where

$$\mathbf{I}=[\mathbf{I}(\tau,\mu_{-N})\ \cdots\ \mathbf{I}(\tau,\mu_N)]^T \quad (26)$$

$$\mathbf{A}_{j,k}=\frac{1}{\mu_j}-\frac{\mathbf{L}(\mu_j,\mu_k)}{\mu_j} \quad (27)$$

$$\mathbf{B}_{j,k}=\frac{\mathbf{F}(\mu_j)}{\mu_j}. \quad (28)$$

In the case of the I_1I_2 equation, $\mathbf{I}$ represents $[I_1\quad I_2]^T$; $\mathbf{L}$ represents $\mathbf{L}_1$; and $\mathbf{F}$ represents $\mathbf{F}_{I_1I2}$. On the other hand, in the case of the UV equation, $\mathbf{I}$ represents $[U\quad V]^T$, $\mathbf{L}$ represents $\mathbf{L}_4$, and $\mathbf{F}$ represents $\mathbf{F}_{UV}$. With the application of the boundary conditions given in (7), we can find the complete solution. The solution is in the discrete angle μ_i, and the accuracy of the solution depends on the number of angles N. However, the required computational resource increases as a function of N because we have to solve the matrix eigen system of order N by N.

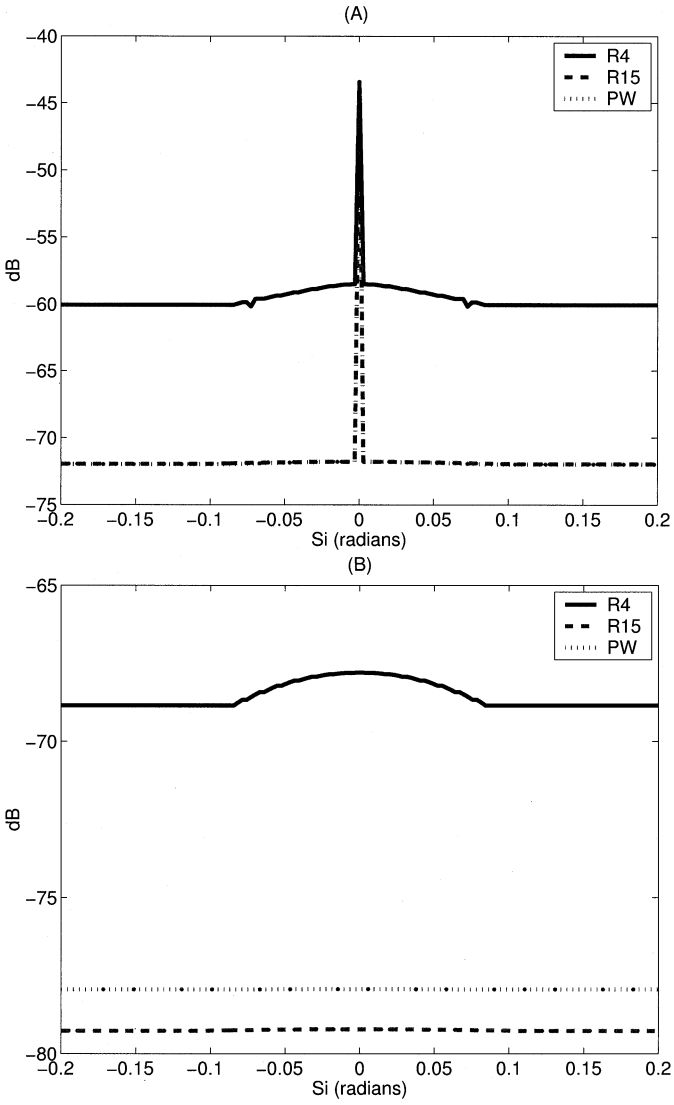

Fig. 8. One-dimensional cut from 2-D point spread function for small distance geometry. (a) Optical depth $= 10$. (b) Optical depth $= 25$.

D. Comparison Between Point-Source and Plane-Wave Incidences

We perform numerical calculations of plane-wave and point-source incidences on a slab of random medium as shown in Fig. 2. The random medium is fog in an air background. We use a wavelength of 1 μm. Fog particles have the size distribution expressed in Table I. The path length (L) of the random medium is 1 km. For the comparison, we calculate the case where the object is close to the slab of random medium ($R_o = 4$ km) with a total length (L_o) of 20 km, and the case where the object is far from the slab of random medium ($R_o = 15$ km) with the same total length as shown in Fig. 3. The calculation is made with optical depths (τ_o) of 10 and 20. The angular spectrums of the copolarized component are compared with those of the plane-wave case, and are shown in Fig. 4. Note that the decibels scale is the logarithm of the intensity calculated at the observation point. The results show the shower curtain effect. In the case when the object is close to the random medium ($R_o = 4$ km), the

angular spectrum is sharper than the case where the object is relatively far from the random medium ($R_o = 15$ km). The results also show that as the distance R_o gets larger, the point-source incidence angular distribution approaches the plane-wave incidence. It is consistent with our assumption, and it is one of the signs that our approximation is valid.

III. Imaging System and the Shower Curtain Effect

As the results from the previous section suggest, the shower curtain effect is evident from the calculation of the point-source radiative transfer equation. Therefore, we consider an imaging system shown in Fig. 5 to investigate the imaging of an object through a random medium. We calculate the point spread function according to the imaging system parameters. We investigate an image of a cross through the random medium in several cases and show the shower curtain effect on these cross images.

A. Point Spread Function

We consider an imaging system with an aperture diameter of D (radius $a = D/2$) and a focal distance of d_i as shown in Fig. 5. In the plane-wave case, the intensity at the imaging plane is given by our previous work [10] as

$$I_i(\bar{s}_i) = \frac{k^2}{(2\pi d_i)^2}(\pi a^2)^2 \left\{ \exp(-\tau_o) \left[\frac{J_1(k\bar{s}_i a)}{\left(\frac{k\bar{s}_i a}{2}\right)} \right]^2 + \frac{1}{\pi}\left(\frac{\lambda}{a}\right)^2 I_{\rm inc}(\bar{s}_i) \right\}$$
$$= \frac{k^2}{(2\pi d_i)^2}\left\{ \exp(-\tau_o) A_i(k\bar{s}_i) + (\pi a \lambda)^2 I_{\rm inc}(\bar{s}_i) \right\} \quad (29)$$

where $\bar{s}_i = \bar{x}_i/d_i$ and $\bar{x}_i = \hat{x}\rho\cos\phi + \hat{y}\rho\sin\phi$. Notice that the first term is the coherent component. The term $A_i(k\bar{s}_i)$ is also called the *Airy pattern* given by

$$A_i(k\bar{s}_i) = \left((\pi a^2) \left[\frac{J_1(k\bar{s}_i a)}{\left(\frac{k\bar{s}_i a}{2}\right)} \right] \right)^2. \quad (30)$$

The coherent component is derived from the diffraction limit, and the resolution is on the order of ka, which is very small. The second term involves the incoherent (diffuse) component. It introduces blurring in the image because its resolution depends on the angular spectrum of $I_{\rm inc}$, which is very coarse, especially when compared with the coherent component.

The point spread function is the total intensity at the imaging plane when a point-source is imaged. The two-dimensional angular point spread function is given by

$$I_i(\bar{s}_i) = \frac{k^2}{(2\pi d_i)^2}(\pi a^2)^2 \left\{ \frac{\exp(-\tau_o)}{L_o^2} \left[\frac{J_1(k\bar{s}_i a)}{\left(\frac{k\bar{s}_i a}{2}\right)} \right]^2 + \frac{1}{\pi}\left(\frac{\lambda}{a}\right)^2 I_{\rm inc}(\bar{s}_i) \right\}. \quad (31)$$

Notice that the coherent component is normalized by L_o^2 because the spherical characteristic of the point-source wave. The aperture size parameter has an effect on the Airy pattern and the amount of incoherent component that incorporates in the point spread function. Also, we will show that the total viewing angle has an effect on the image. Therefore we consider the following two cases of imaging conditions. First, we consider a large distance and small angle imaging. The geometry of this imaging problem is shown in Fig. 6(a). The aperture size (D) is 3 cm and the focal distance (d_i) is 50 cm. The viewing angle is in milliradian range. This geometry corresponds to the telescopic viewing of an object at a long distance. Second, we discuss the small distance and large angle imaging geometry shown in Fig. 6(b). The aperture size in this case is 3 mm with a focal distance of 1.6 cm. The viewing angle is in the radian range. This geometry represents human observation of a relatively near object. We calculate the point spread function using (31), and the result are presented in Figs. 7 and 8. Fig. 7 shows the point spread function of the large distance geometry in the coherent dominant and incoherent dominant cases. We show the point spread function in the decibels scale where 0 dB represents the level of coherent component if there is no random medium. In the case of optical depth of ten, we can see that the peak of the point spread function is at about -43 dB, which corresponds to the $\exp(-10)$ reduction factor. The point spread function consists of the airy pattern and angularly flat incoherent component behaving like a noise. Based on (31), the coherent part of the point spread function explicitly depends on the distance L_o. In our calculations, the level of the coherent component in the case of small R_o is higher than the case of large R_o. It is because the intensity incidence on the random medium in the case of small R_o is larger. However, the plot shows that their amplitudes are equal. It is because we normalized the intensity with the distance to illustrate the effect of distance on the diffuse component.

At a large optical depth, the incoherent component dominates. Therefore, the Airy pattern is submerged and the point spread function is flat. In contrast, Fig. 8 shows the point spread function of the small distance geometry. Because the viewing angle is large, the point spread function is a combination of the Airy pattern, which is approximately a single peak, and the incoherent component which exhibits a dome shape. Again, at a large optical depth, the incoherent component is predominant. The angular sharpness is obvious in this case and leads to the shower curtain effect.

The results suggest that we can consider the imaging in two conditions: coherent dominated and incoherent dominated. In the coherent dominated regime, the point spread function approaches the diffraction limit and the scattering produces the diffuse component, which acts like a noise. The contrast of the image is impaired by this diffuse component where the images still retains its resolution. Therefore, the resolution of the image depends heavily on the size of the aperture and the wavelength because the resolution in diffraction limit is proportion to λ/D. In the incoherent dominated regime, the resolution of the image reduced drastically. The angular spectrum of the diffuse component governs the image quality. In this case, the scattering characteristics of the medium have strong effects on the resolution of the image. Therefore, in the discrete particles environment that we consider, the particle size is the important factor in determining the resolution.

B. Shower Curtain Effect on Cross Images

We perform numerical simulations to illustrate the effect of the random medium. Cross patterns shown in Fig. 9 are imaged

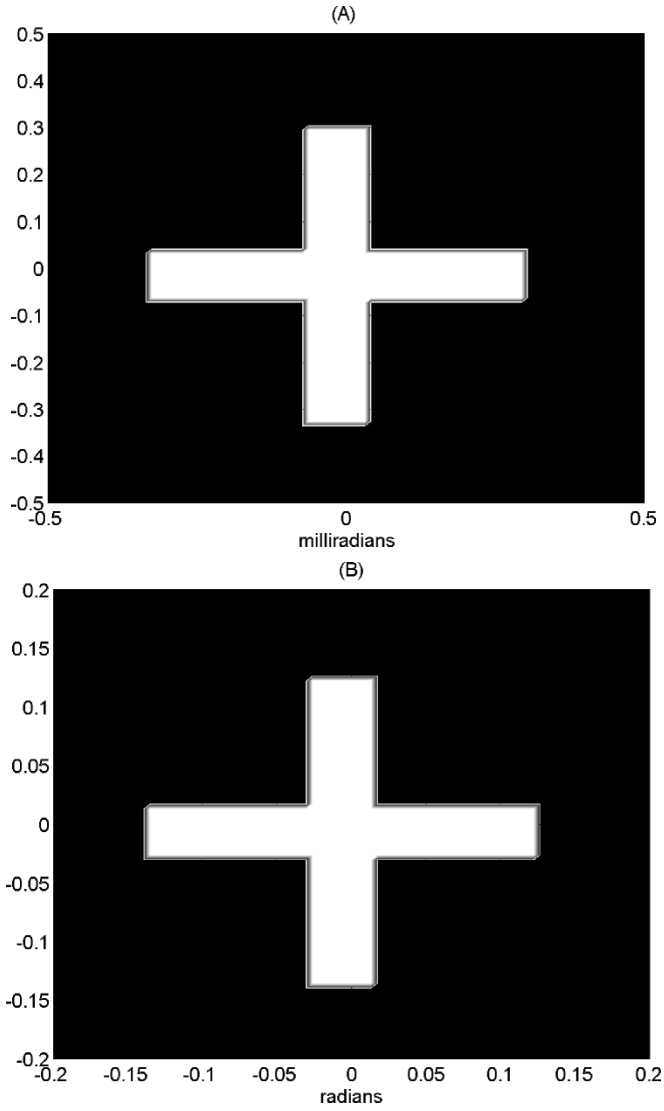

Fig. 9. Cross images for (A) large distance geometry and (B) small distance geometry.

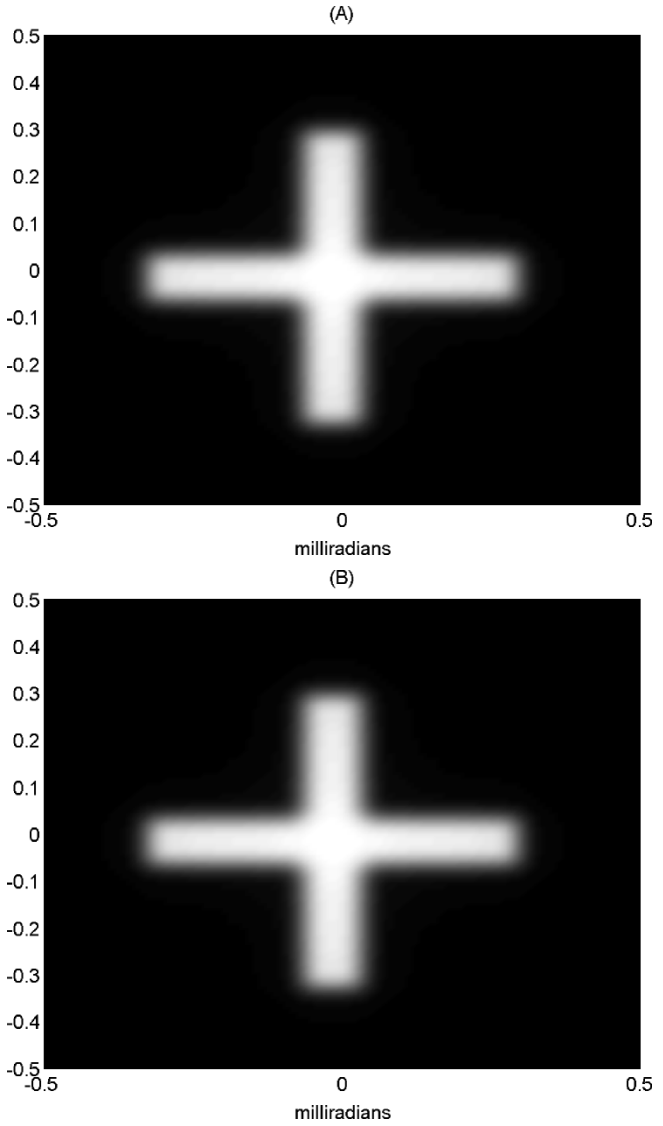

Fig. 10. Cross image through a random medium of optical depth 10 in the large distance geometry. (a) $R_o = 15$ km. (b) $R_o = 4$ km.

through a random medium with different geometries explained in the previous section. We base our calculations on convolution of point spread function calculated by (31) with the cross pattern. The results are the intensity at the imaging plane under the assumption that the detectors are infinitely small. These simulations assume that the dynamic range is not limited and there is no noise. As the point spread function results shown in the Figs. 7 and 8, the dynamic range needed for the case of optical depth of 10 is about 30 dB. These assumptions of infinitely small detector, no noise, and unlimited dynamic range facilitate us to concentrate on the effect of random media alone. When the detector size is involved, the received power at each detectors is considered instead of the intensity. All the cross pattern images are normalized to their respective maximum values. They are scaled to the same range of zero to 100 for a fair comparison, where 100 represents the white color.

For the large distance geometry, the cross image corresponds to the size of 20 m at the object plane and 0.5 mm at the image plane assuming the focal length (d_i) is 50 cm. For the small distance geometry, the cross image corresponds to the size of 0.8 mat the object plane and 6.3 mm at the image plane assuming the focal length (d_i) is 1.6 cm. For large distance geometry, we express the results in Fig. 10 and in the case of optical depth of 10. For small distance geometry, the results are exhibited in Figs. 11 and 12 for the cases of optical depth of 10 and 25, respectively.

In the large distance geometry shown in Fig. 10, we observe only a small viewing angle. Within this angle, we only see the variation due to the Airy pattern. The incoherent component in our calculation is a constant. Therefore, the image is formed by mostly the coherent component with a background from the incoherent component. When the optical depth is small, the coherent component contributes more to the images. Thus, the resolution of the image is on the order of the Airy pattern, which is very small. The incoherent component can be considered as a background noise at very small resolution. As a result, the cross image still shows a good cross pattern with the contrast depending on the level of background noise. For a large optical

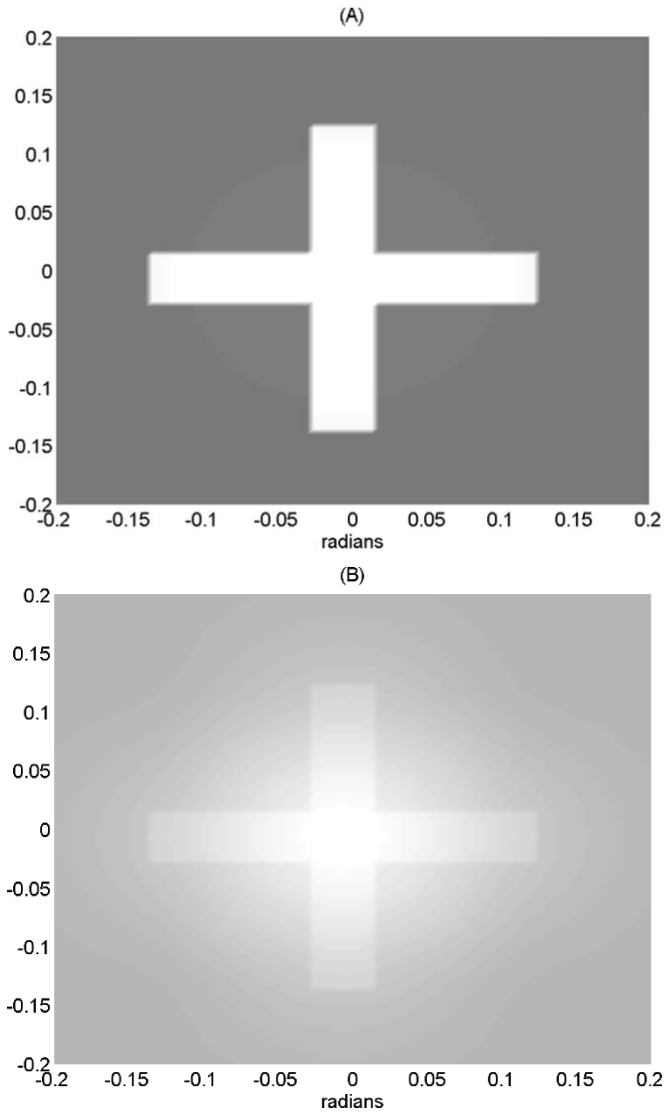

Fig. 11. Cross image through a random medium of optical depth 10 in the small distance geometry. (a) $R_o = 1.5$ m. (b) $R_o = 0.4$ m.

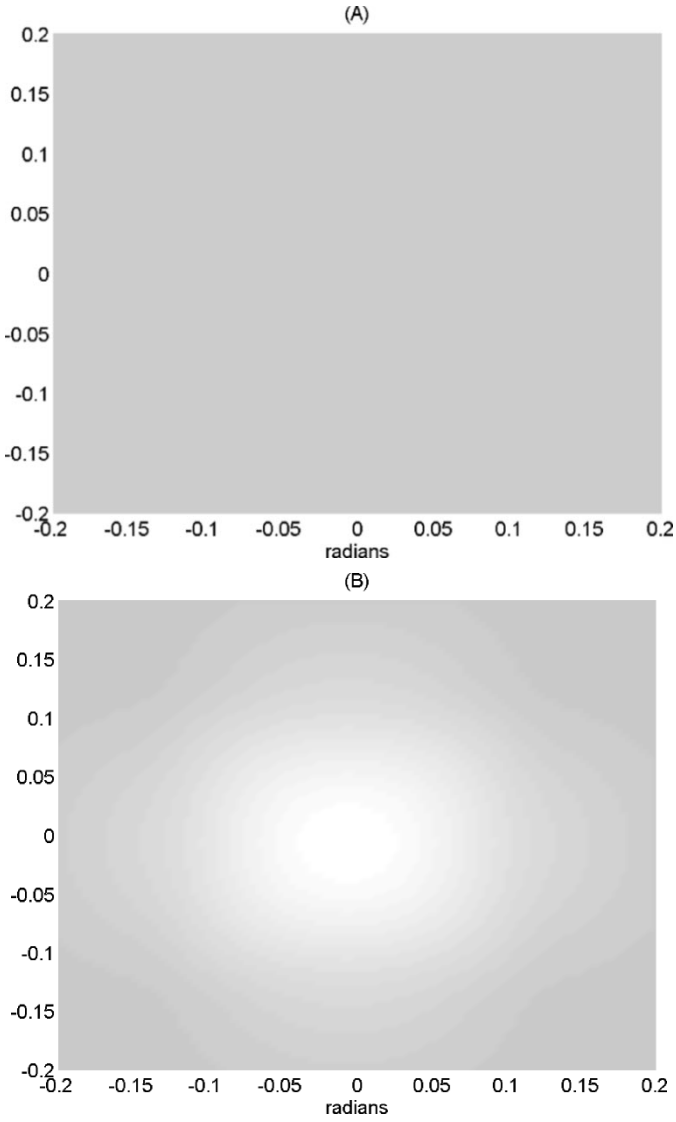

Fig. 12. Cross image through a random medium of optical depth 25 in the small distance geometry. (a) $R_o = 1.5$ m. (b) $R_o = 0.4$ m.

depth, we have calculate the cross images for an optical depth of 25. We found that the cross images disappear in all distance cases. It is because the flat point spread function resulting from domination of the incoherent component. Thus, we do not show the cross images in this case.

For the case of small distance geometry, we view the large angle. The point spread function behaves as a two-dimensional delta function with a background from the incoherent component with a flatter background in the case of larger R_o. For a small optical depth as shown in Fig. 11, the coherent component is dominant. Therefore, the cross image still has good resolution. On the other hand, in Fig. 12 when the large optical depth case is considered, the incoherent component dominates. Therefore, the resolution of the image depends on the angular resolution of the diffuse intensity at the imaging plane from the solution of the radiative transfer. The cross image in the case of large R_o is almost invisible. However, in the small R_o case, we can still see some trace of the cross image because the angular spectrum of it is sharper. This sharpness at small R_o is the evidence of the shower curtain effect. This shows that when scattering is dominant (optical depth is large), the case of small distance between the object and the random medium (small R_o) provides a better image than the case of large distance between the object and the random medium (large R_o).

From the result, we can conclude that the shower curtain effect is strong in the incoherent dominating region , i.e., optical depth is large. Also, large viewing angles are desired to demonstrate the shower curtain effect since we base our calculations on the radiative transfer equation which provides very little information for the small angles close to optical axis. However, we believe that the images would show the shower curtain effect in small viewing angles too. In other words, the point spread function for the case of small distance between the source and medium would be sharper than the case of large distance between the source and medium.

IV. Conclusion

We derive the point-source vector radiative transfer equation in plane parallel geometry using the formulation of plane-wave

incidence with some assumptions. Using the discrete ordinates method, we are able to transform an integrodifferential form of the radiative transfer equation into a first-order differential equation, which is solved by imposing the boundary conditions. Then, we compare the angular spectrum of the plane-wave case to the point-source case with different distances between the object and the slab of the random medium. Furthermore, we study the point spread function of an imaging system. We show that there are two cases under consideration, which are the coherent dominant and incoherent dominant. Cross patterns are imaged through the random medium, and the results show that the shower curtain effect is evident in the case of large optical depth when the incoherent component is dominant.

APPENDIX

The scattering amplitudes for the spherical particles are given by

$$f_{11} = (l,l)T_1 + (r,r)T_2 \tag{32a}$$
$$f_{12} = -(r,l)T_1 + (l,r)T_2 \tag{32b}$$
$$f_{21} = -(l,r)T_1 + (r,l)T_2 \tag{32c}$$
$$f_{22} = (r,r)T_1 + (l,l)T_2 \tag{32d}$$

where

$$(l,l) = \left[(1-\mu^2)(1-\mu'^2)\right]^{1/2} + \mu\mu'\cos(\phi'-\phi) \tag{33a}$$
$$(l,r) = -\mu'\sin(\phi'-\phi) \tag{33b}$$
$$(r,l) = \mu'\sin(\phi'-\phi) \tag{33c}$$
$$(r,r) = \cos(\phi'-\phi) \tag{33d}$$
$$T_1(x) = \frac{A_{rr}(\chi) - \chi A_{ll}(\chi)}{1-\chi^2} \tag{33e}$$
$$T_2(x) = \frac{A_{ll}(\chi) - \chi A_{rr}(\chi)}{1-\chi^2} \tag{33f}$$
$$\chi = \cos\Theta = [(1-\mu^2)(1-\mu'^2)]^{1/2}\cos(\phi'-\phi) + \mu\mu' \tag{33g}$$
$$\mu = \cos(\theta), \mu' = \cos(\theta'). \tag{33h}$$

(θ,ϕ) and (θ',ϕ') corresponds to the incident and scattered wave directions, respectively. The function A_{ll} and A_{rr} is related to the scattering function s_1 and s_2 for Mie solution explained by Van de Hulst [7] as

$$A_{ll} = \frac{is_2^*}{k} \quad A_{rr} = \frac{is_1^*}{k} \tag{34}$$

ACKNOWLEDGMENT

The author thanks C. Mason (U.S. Air Force Research Laboratory) for many discussions, comments, and suggestions.

REFERENCES

[1] V. V. Belov and B. D. Borisov, "T-effect and "shower curtain" effect," *Proc. SPIE*, vol. 4338, pp. 8–16, 2000.

[2] Y. Kuga and A. Ishimaru, "Modulation transfer function of layered inhomogeneous random media using the small-angle approximation," *Appl. Opt.*, vol. 25, pp. 4382–5, 1986.

[3] P. Bruscaglioni, P. Donelli, A. Ismaelli, and G. Zaccanti, "Inhomogeneity of turbid media and its effect on the MTF of an optical system," *Nuovo Cimento D*, vol. 15, pp. 775–83, 1993.

[4] I. Dror, A. Sandrov, and N. S. Kopeika, "Experimental investigation of the influence of the relative position of the scattering layer on image quality: The shower curtain effect," *Appl. Opt.*, vol. 37, pp. 6495–9, 1998.

[5] L. Thrane, H. T. Yura, and P. E. Anderson, "Analysis of optical coherence tomography systems based on the extended Huygens-Fresnel principle," *J. Opt. Soc. Amer.*, vol. A-17, pp. 484–90, 2000.

[6] A. Tycho, T. M. Joergensen, and L. Thrane, "Focusing problem in OCT: Comparison of Monte Carlo simulations, the extended Huygens-Fresnel principle, and experiments," *Proc. SPIE*, vol. 3915, pp. 25–35, 2000.

[7] H. C. Van de Hulst, *Light Scattering by Small Particles*. New York: Wiley, 1957.

[8] A. Ishimaru, S. Jaruwatanadilok, and Y. Kuga, "Polarized pulse waves in random discrete scatterers," *Appl. Opt.*, vol. 40, pp. 5495–502, 2001.

[9] I. B. George and S. Glasstone, *Nuclear Reactor Theory*: Robert E. Krieger, 1979.

[10] S. Jaruwatanadilok, A. Ishimaru, and Y. Kuga, "Photon density wave for imaging through random media," *Waves Random Media*, vol. 12, pp. 351–364, 2002.

[11] A. Ishimaru, *Wave Propagation and Scattering in Random Media*. Piscataway, NJ: IEEE Press, 1997.

Sermsak Jaruwatanadilok received the B.E. degree in telecommunication engineering from King Mongkut's Institute of Technology Ladkrabang, Thailand, in 1994, the M.S. degree in electrical engineering from Texas A&M University, College Station, in 1997, and the Ph.D. degree in electrical engineering from the University of Washington, Seattle, in 2003.

He is currently with the University of Washington. His research interests are optical wave propagation and imaging in random medium, as well as optical and microwave remote sensing

Akira Ishimaru (M'58–SM'63–F'73–LF'94) received the B.S. degree from the University of Tokyo, Tokyo, Japan, in 1951, and the Ph.D. degree in electrical engineering from the University of Washington, Seattle, in 1958.

From 1951 to 1952, he was with the Electrotechnical Laboratory, Tanashi, Tokyo, and in 1956, he was with Bell Laboratories, Holmdel, NJ. In 1958, he joined the Department of Electrical Engineering, University of Washington, where he was a Professor of electrical engineering and an Adjunct Professor of applied mathematics. He is currently Professor Emeritus there. He has also been a Visiting Associate Professor at the University of California, Berkeley. His current research includes waves in random media, remote sensing, object detection, and imaging in clutter environment, inverse problems, millimeter wave, optical propagation and scattering in the atmosphere and the terrain, rough surface scattering, and optical diffusion in tissues. He is the author of *Wave Propagation and Scattering in Random Media* (NewYork: Academic, 1978; IEEE-Oxford University Press Classic reissue, 1997) and *Electromagnetic Wave Propagation, Radiation, and Scattering* (Englewood Cliffs, NJ: Prentice-Hall, 1991). He was Editor (1979–1983) of *Radio Science* and Founding Editor of *Waves in Random Media*.

Dr. Ishimaru was a Member-at-Large of the U.S. National Committee (USNC) and was Chairman (1985–1987) of Commission B of the USNC/International Union of Radio Science. He is a Fellow of the Optical Society of America, the Acoustical Society of America, and the Institute of Physics, U.K. He was the recipient of the 1968 IEEE Region VI Achivement Award and the IEEE Centennial Medal in 1984. He was appointed as Boeing Martin Professor in the College of Engineering in 1993. In 1995, he was awarded the Distinguished Achievement Award from the IEEE Antennas and Propagataion Society. He was elected to the National Academy of Engineering in 1996. In 1998, he was awarded the Distinguished Achievement Award from the IEEE Geoscience and Remote Sensing Society. He is the recpient of the 1999 IEEE Heinrich Hertz Medal and the 1999 URSI Dellinger Gold Medal. In 2000, he received the IEEE Third Millennium Medal.

Yasuo Kuga (S'79–M'83–SM'90) received the B.S., M.S., and Ph.D. degrees from the University of Washington, Seattle, in 1977, 1979, and 1983, respectively.

He is currently a Professor of electrical engineering at the University of Washington. From 1983 to 1988, he was a Research Assistant Professor of electrical engineering at the University of Washington. From 1988 to 1991, he was an Assistant Professor of electrical engineering and computer science at the University of Michigan, Ann Arbor. Since 1991, he has been with the University of Washington. He was an Associate Editor of *Radio Science* (1993–1996). His research interests are in the areas of microwave and millimeter-wave remote sensing, high-frequency devices, and optics.

Dr. Kuga is an Associate Editor of the IEEE TRANSACTIONS ON GEOSCIENCE AND REMOTE SENSING (1996–2000). He was selected the 1989 Presidential Young Investigator.